9-2014

The Critical Role of Water at the Gold-titania Interface in Catalytic CO Oxidation

Johnny Saavedra
Trinity University, jsaaved1@trinity.edu

Hieu Doan
University of Houston - Main

Christopher J. Pursell
Trinity University, cpursell@trinity.edu

Lars C. Grabow
University of Houston - Main

Bert D. Chandler
Trinity University, bchandle@trinity.edu

CATALYSIS

The critical role of water at the gold-titania interface in catalytic CO oxidation

Johnny Saavedra,[1] Hieu A. Doan,[2] Christopher J. Pursell,[1] Lars C. Grabow,[2]* Bert D. Chandler[1]*

We provide direct evidence of a water-mediated reaction mechanism for room-temperature CO oxidation over Au/TiO_2 catalysts. A hydrogen/deuterium kinetic isotope effect of nearly 2 implicates O-H(D) bond breaking in the rate-determining step. Kinetics and in situ infrared spectroscopy experiments showed that the coverage of weakly adsorbed water on TiO_2 largely determines catalyst activity by changing the number of active sites. Density functional theory calculations indicated that proton transfer at the metal-support interface facilitates O_2 binding and activation; the resulting Au-OOH species readily reacts with adsorbed Au-CO, yielding Au-COOH. Au-COOH decomposition involves proton transfer to water and was suggested to be rate determining. These results provide a unified explanation to disparate literature results, clearly defining the mechanistic roles of water, support OH groups, and the metal-support interface.

The interactions between transition-metal nanoparticles and their metal-oxide supports are often critical for heterogeneous metal nanoparticle catalysts (*1*). However, the roles of the species involved are often not well understood, especially for supported Au catalysts, which are active for selective hydrogenations (*2*, *3*), oxidations (*3*–*5*), and the water-gas shift (WGS) reaction (*3*, *6*). Several factors have been suggested for the exceptionally high activity of Au catalysts, including quantum size effects (*7*), particle geometry (*8*, *9*), and undercoordinated Au atoms (*10*–*12*).

Oxygen activation at the metal-support interface is widely regarded as the key step in room-temperature CO oxidation (*13*–*17*), but substantial debate remains regarding the nature of the active site (*9*, *12*, *17*–*23*). Experimental studies indicate that materials lacking OH groups are inactive (*24*, *25*), yet, the dominant mechanistic models vary in the suggested role of support OH groups and generally highlight the possible role of oxygen vacancies (*16*, *17*, *22*–*24*, *26*). Computational models also have not indicated a clear mechanistic role for the support OH groups, and isotope-labeling studies indicate that CO and O_2 react without incorporating oxygen from the support (*21*, *27*). Perhaps most importantly, as Fig. 1A shows, water markedly increases catalytic activity (*20*, *21*, *26*, *27*), yet only one proposed mechanism suggests a direct potential role for water (*21*).

We performed an experimental and computational study to better understand how water, surface hydroxyls, and the metal-support interface interact during CO oxidation over Au/TiO_2 catalysts. The surface water and hydroxyl groups of a commercial Au/TiO_2 catalyst were deuterated in situ with flowing D_2O/N_2 [supplementary materials (SM) 3.1 and 3.2]. The exchanged catalyst was then flushed with N_2 to remove excess D_2O. Under these conditions, we measured a large kinetic isotope effect (KIE, k_H/k_D = 1.8 ± 0.1, Fig. 1B), consistent with a primary KIE, indicating O-H(D) bond cleavage in the rate-determining step (RDS). Previous studies on Au/Al_2O_3 catalysts (*21*, *28*) found almost no rate difference ($k_H/k_D \approx 1$ to 1.2) upon switching H_2O for D_2O in the feed and concluded that an equilibrium isotope effect might be involved (*21*). Our studies (Fig. 1C) showed that adding 700-Pa H_2O/D_2O to the feed reduced the observed KIE to 1.4. This change was reversible: 60 min after removing H_2O/D_2O from the feed, the KIE approached the original value (Fig. 1C). The large KIE under relatively dry conditions indicates that water or support OH must be involved in the reaction mechanism and that O-H(D) bond cleavage occurs in a kinetically important step. Further, the reaction is subject to saturation kinetics, with added water affecting the kinetics of the RDS.

We explored potential mechanistic roles of O-H bonds with density functional theory (DFT) studies using a 10-atom gold nanocluster residing on four layers of TiO_2(110) support. Unlike previous studies, our computational model (SM 2.5 and 2.6) includes both support OH groups and adsorbed water (*13*, *14*, *18*, *29*). This model substantially simplifies the real system, using a small Au cluster and a single water molecule to represent 3-nm particles and multiple water molecules. Thus, the DFT calculations provide substantial insight into likely elementary reaction steps, but need to be interpreted in the context of the more complex real system.

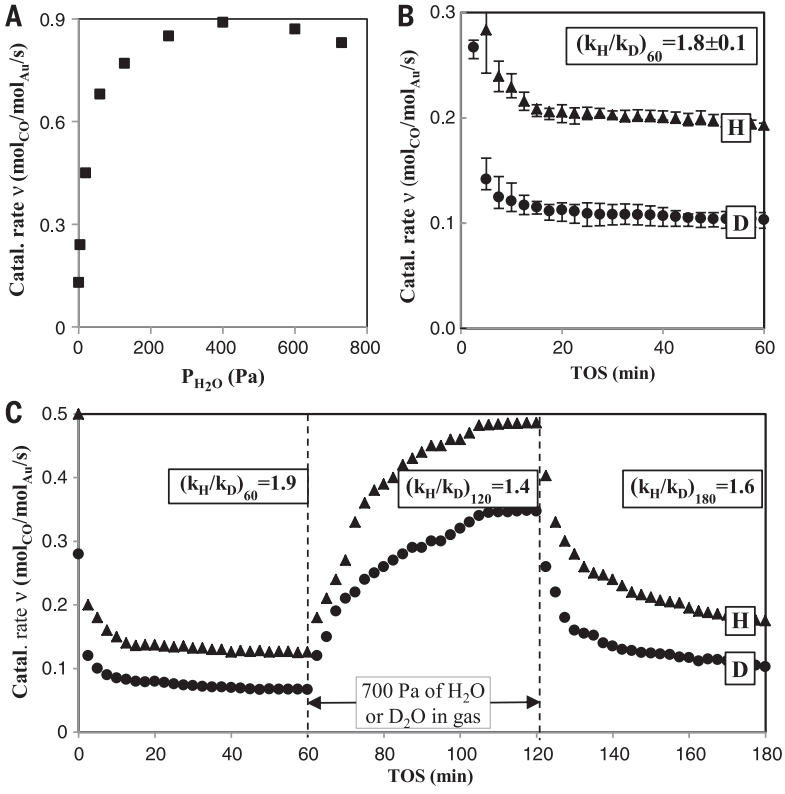

Fig. 1. Water and kinetic isotopic effects on CO oxidation over Au/TiO_2. (**A**) Effects of water on the overall reaction rate. (**B**) Reaction rate for protonated (▲**H**) and deuterated (•**D**) catalysts in the absence of added water (six trials averaged). (**C**) Changes in reaction rate induced by adding 700 Pa of H_2O/D_2O. Reaction conditions: 20°C, 1% CO, 20% O_2, space velocity (SV) = 36 liters g catalyst^{-1} min^{-1}.

[1]Department of Chemistry, Trinity University, San Antonio, TX 78212-7200, USA. [2]Department of Chemical and Biomolecular Engineering, University of Houston, Houston, TX 77204-4004, USA.
*Corresponding author. E-mail: bert.chandler@trinity.edu (B.D.C.); grabow@uh.edu (L.C.G.)

The H_2O molecule adsorbed on a bridging OH group at the metal-support interface through hydrogen bonding interactions; this adsorption motif was ~1.0 eV more stable than adsorption on the Au cluster and ~1.4 eV more stable than adsorption on a bridging OH group away from the interface (SM 6.1). Although we studied several O_2 adsorption and activation pathways (Fig. 2, SM 6.2 and 6.3), we did not find an intermediate species with O_2 bound only to Au atoms near the metal-support interface. In all cases, an essentially barrier-free proton transfer lowered the overall energy of the system, generating H_2O_2* or *OOH (Fig. 2; "*" references species adsorbed to Au). Once *OOH formed, it migrated along the Au particle, allowing atoms near, but not strictly at, the metal-support interface to participate in the reaction.

The KIE and DFT studies indicate proton transfer in a key reaction step, but they do not provide sufficient information to determine if the reaction is initiated by adsorbed water or support OH groups. In situ infrared spectroscopy was therefore used to quantify these species (SM 4.1) and compare catalyst activity to their relative surface concentrations. The non–hydrogen-bonded ν_{OH} stretching vibration centered near 3650 cm^{-1} is exclusively associated with support OH groups, whereas the δ_{HOH} bending vibration centered at 1623 cm^{-1} is exclusively due to adsorbed water. There is also a broad band centered around 3400 cm^{-1} assigned to ν_{OH} for OH groups involved in hydrogen bonding that may have contributions from both water and Ti-OH [complete infrared (IR) analysis in SM 4.1].

Our catalysis studies do not indicate a direct role for support OH groups in the reaction mechanism. Gentle drying with flowing N_2 (Table 1 and Fig. 3A) only removed water and had little effect on the support OH bands. Catalytic activity, however, dropped by an order of magnitude, indicating that adsorbed water, not support OH, is the key proton donor. Further, a constrained ab initio thermodynamic analysis (SM 2.6) indicates that the support OH groups at the metal-support interface are thermodynamically unstable relative to gas-phase water under dry conditions and therefore would be unavailable as proton donors. As water is added to the system, the interfacial support OH groups and weakly adsorbed water are equilibrated and ultimately become indistinguishable.

Several mechanisms reported in the literature invoke OH transfer from the support to Au (*17*, *23*) as an elementary step. Our experimental and DFT studies do not support such a step. The calculated barrier for transferring a Ti^{cus}-OH group to Au [activation energy (E_a) = 1.63 eV, SM 6.5] is too large to be a viable room-temperature pathway. Further, generating *COOH from *CO and *OOH (ΔE = –2.23 eV, E_a = 0.10 eV) is thermodynamically and kinetically far more favorable than the reaction between *CO and Ti^{cus}-OH (ΔE = 0.60 eV, E_a = 0.72 eV, SM 6.5).

To quantify the effects of adsorbed water, we performed a series of adsorption, thermogravimetric analysis (TGA), and kinetics experiments. IR spectroscopy showed water adsorption on titania (not on Au, SM 4.1), consistent with DFT calculations (SM 6.1). The adsorption isotherm quasi-saturated around 700 Pa (1.7 weight %, 13 molecules/nm^2), corresponding to roughly 1.5 monolayers of water on titania, suggesting a bilayer adsorption structure typical for water (*30*). The reaction rate correlates extremely well with the amount of weakly adsorbed water, and the reaction order (1.33, Fig. 3B) is substantially larger than the reaction orders for CO or O_2 (0.01 and 0.1 to 0.3, respectively; SM 5.1 to 5.3).

We further evaluated the reaction kinetics using a Michaelis-Menten (M-M) kinetic model (SM 5.2), which provides quantitative metrics that characterize heterogeneous catalysts (*31*). This model helps distinguish between changes in the inherent activity of the active site (measured with K_R—analogous to the conventional K_M) and the relative number of active sites (associated with ν_{max}). Double-reciprocal plots of the O_2 dependence data (Fig. 3C) yield K_R values that are independent of the water coverage (Fig. 3D), indicating that H_2O did not affect the inherent reactivity of the active sites. The ν_{max} values, however, increased linearly with adsorbed water. Because K_R was essentially constant, this indicates that weakly adsorbed water increased the effective number of active sites rather than changing their inherent reactivity.

Two explanations for increasing the number of active sites are consistent with the DFT studies and recognize the importance of the metal-support interface (*9*, *12*, *18*–*23*). First, if oxygen binding requires protons from weakly adsorbed water, then increasing the water coverage should increase the number of available protons and facilitate O_2 binding. Second, the DFT studies suggest that *OOH can interact with Au atoms that are near, but not strictly at, the metal-support interface. As additional Au sites gain access to protons from water, a greater number of O_2/peroxo-binding sites become available. This increase in active-site density also argues strongly against O atom vacancies on the support being the active sites for O_2 activation, as surface water would be expected to rapidly fill those vacancies.

The conclusion that support OH groups do not directly participate in the reaction mechanism requires a new model to explain why the support and surface OHs strongly influence CO oxidation activity (*13*–*15*, *24*, *25*). Our results indicate that the support OH groups' primary role is to anchor active water near the Au particle and possibly help activate it through hydrogen bonding. The relative number of support OHs near Au particles and their ability to anchor enough water to facilitate the reaction may partially explain the strong support effects reported in the literature (*3*, *17*, *22*, *23*).

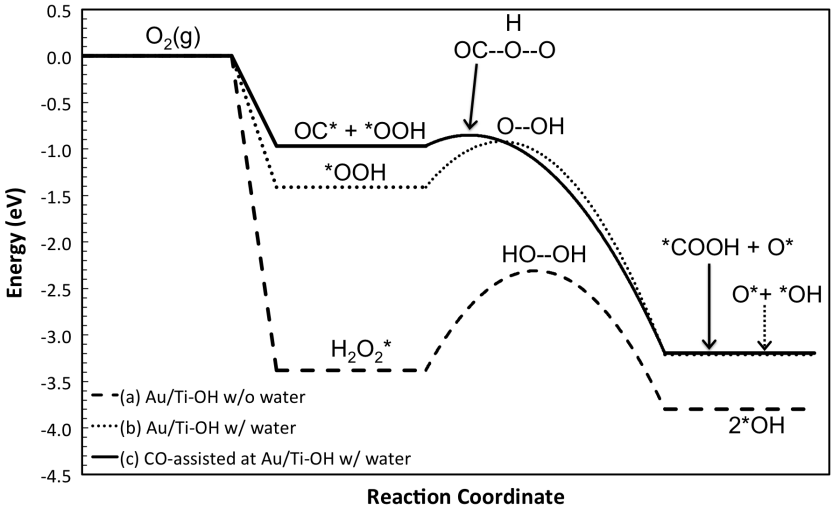

Fig. 2. Potential energy diagrams for O_2 binding and O-O bond activation near the Au/TiO_2 interface. (a): In the absence of H_2O (dashed pathway), O_2 adsorption at the Au/TiO_2 interface initiates a spontaneous transfer of two protons, forming H_2O_2*; (b): with an adsorbed H_2O (dotted pathway), O-O bond activation leads preferentially to O* and *OH; (c): with adsorbed H_2O and CO (solid pathway), O-O scission is facilitated by nucleophilic attack of *CO, resulting in *COOH (carboxyl).

Table 1. Effects of drying treatments on IR spectra and catalytic activity.

Drying treatment*	Ti-OH area†	H_2O area‡	υ (s^{-1})
None	14.3	842	0.32
20°C, 0.5 hour	14.1	503	0.22
70°C, 0.5 hour	14.0	228	0.18
20°C, 16 hours	13.9	131	0.09
70°C, 16 hours	13.8	102	0.03

*N_2 flowing at 50 ml/min. †3741–3645 cm^{-1}. ‡3800–1800 cm^{-1}.

Although the DFT results for O_2 adsorption are congruent with proton transfer as part of the mechanism, they do not explain the observed KIE. The *OOH species have moderate direct decomposition barriers (E_a ~0.5 eV, Fig. 2 and SM 6.3). However, CO-assisted *OOH activation yielding *O and *COOH was found to be extremely facile (E_a = 0.10 eV, Fig. 2). This O-OH dissociation barrier is lower than the previously reported barriers for the related CO-assisted O_2* dissociation on supported and unsupported Au clusters (*10*, *13*, *14*, *18*, *32*). In contrast to the predominant opinion reported in the literature (*16*), the extremely low barriers associated with this pathway suggest that O_2 activation is quite facile in the presence of water and CO.

To explain the observed KIE and close the catalytic cycle, we explored possible *COOH decomposition pathways (SM 6.6); Fig. 4 shows the two most relevant pathways. In the first pathway, the proton is spontaneously transferred from *COOH to the coadsorbed O* (green, ΔE = –0.27 eV, E_a = 0.0 eV), leaving *OH on the surface after CO_2 desorption. Closing the catalytic cycle requires the direct reaction between *OH and *CO (ΔE = 0.10 eV, E_a = 0.40 eV, SM 6.4) to yield *COOH, followed by *COOH decomposition, which returns the proton and restores the active site. The second pathway is initiated by an endothermic proton transfer from *COOH to an adsorbed water molecule (simultaneously transferring a proton to the support) (purple, ΔE = 0.61 eV; E_a = 0.76 eV), followed by CO_2 desorption. The remaining O* reacts with *CO in a well-studied reaction (ΔE = –1.03 eV; E_a = 0.65 eV, SM 6.4).

These pathways are chemically similar, differing primarily in the order of the steps. The reactions between *CO and *O or *OH have fairly similar barriers, and both pathways also go through the same endothermic *COOH decomposition step. This step is the likely RDS because it involves a proton transfer (*COOH to water) and has the highest computed activation-energy barrier (movie S1). DFT calculations based on this transition state (involving a single water molecule) yielded a calculated KIE of 2.55 (SM 6.7), which represents an upper limit to the experimentally determined KIE at low water coverage. The predicted lower limit of the equilibrium isotope effect associated with this step is 1.08. This is somewhat lower than the value we measured at 700-Pa water, but is similar to low values previously reported using higher water pressures (*21*, *28*).

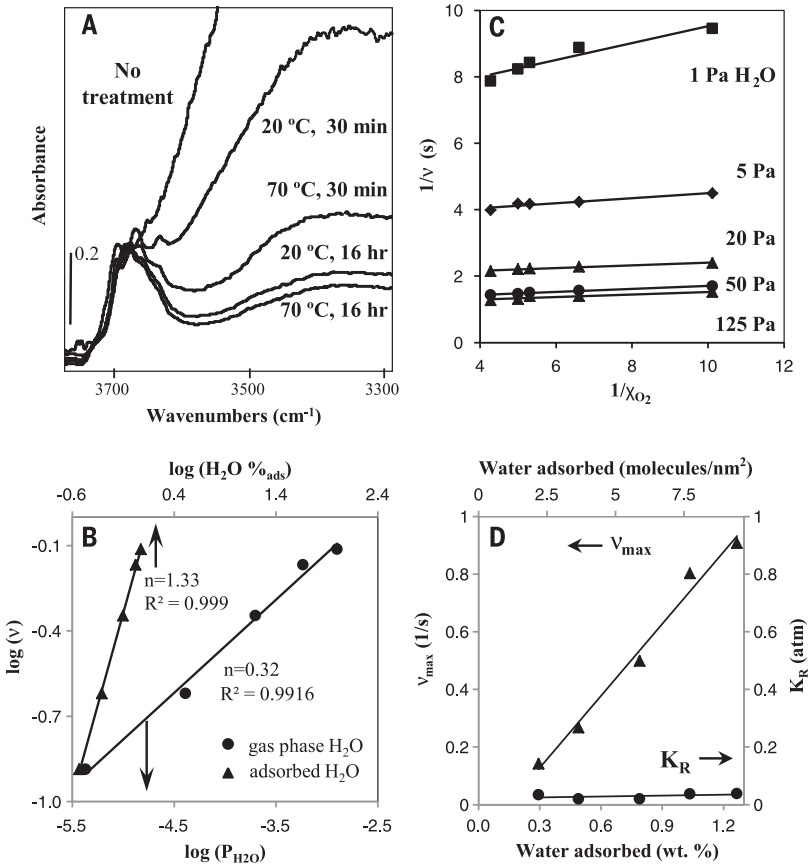

Fig. 3. Infrared spectroscopy and kinetics data showing the changes associated with weakly adsorbed water. (**A**) IR spectra and treatment conditions for gently dried catalysts. (**B**) Reaction order based on gas phase (•) and weakly adsorbed (▲) water (20°C, 1% CO, 20% O_2, SV = 35 liters g catalyst^{-1} min^{-1}). (**C**) Double-reciprocal plots used in Michaelis-Menten kinetic treatment. (**D**) Michaelis-Menten kinetic parameters versus catalyst water content.

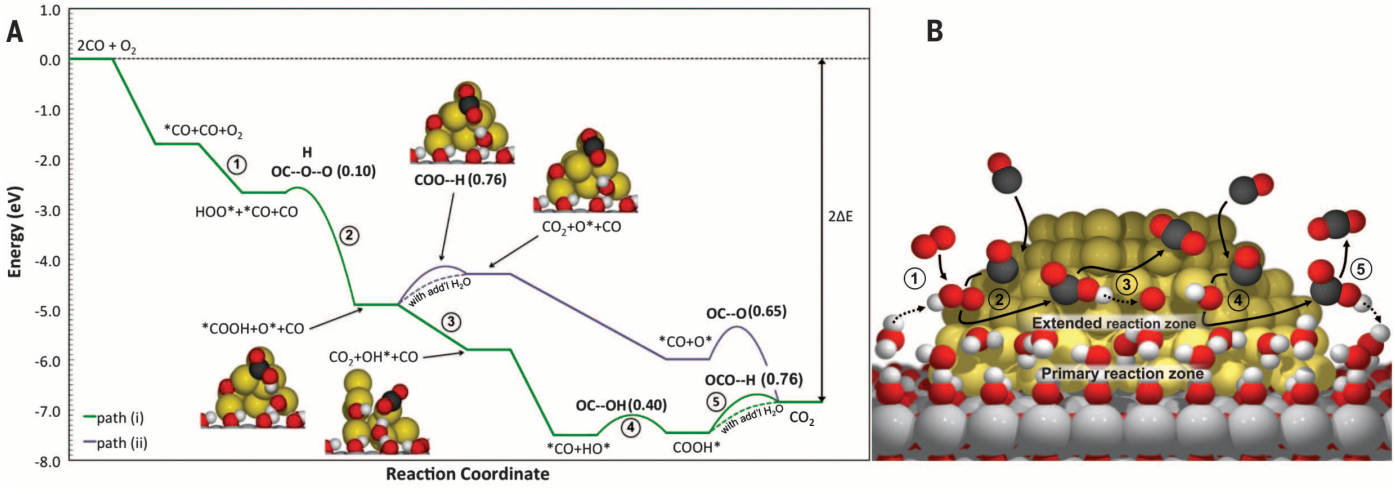

Fig. 4. Proposed reaction mechanism. (**A**) Potential energy diagram; both pathways are limited by a combination of *COOH decomposition and the reaction between *CO and *O(H). (**B**) Schematic representation of the lower (green) pathway.

The involvement of weakly adsorbed water in multiple mechanistic steps is also consistent with the large reaction order (1.3). DFT calculations also indicate that a second adsorbed water molecule in the vicinity of the *COOH species facilitates the proton transfer, which only needs to overcome the thermodynamic barrier (ΔE = 0.70 eV, E_a = 0.70 eV, SM 6.6). Further, at higher water coverage, rapid proton mobility (*33*) can explain the shift to an equilibrium isotope effect. *COOH decomposition has also been identified as the RDS in the related WGS reaction on Cu and Pt (*34*, *35*), and this elementary step is consistent with reports of NaOH promoting CO oxidation over Au catalysts (*17*, *36*).

The CO oxidation mechanism shown in Fig. 4, along with the structural model of support OH groups anchoring and activating water near Au particles, provides a fresh framework for interpreting previous results. This model provides a single active-site description that unifies some very disparate mechanistic information, accounts for the promotional effects of water, and is consistent with previously reported isotope exchange studies (*21*, *27*) that indicate that CO and O_2 must react directly on the Au particles without exchanging O atoms with the support or adsorbed water. At the same time, it maintains the importance of the support OH groups and the metal-support interface without directly involving them in the reaction mechanism. The likely active sites bear a strong resemblance to the WGS mechanism over Au catalysts, where the support anchors water near Au-CO sites (*6*).

This proposed mechanism explains why the O_2 adsorption and activation steps, which are widely regarded as the critical mechanistic steps, have been so difficult to characterize. The fast room-temperature catalysis mechanism requires both water and CO for O_2 binding and activation. Experiments performed without water, particularly ultrahigh-vacuum and DFT studies, ultimately probe different reaction mechanisms than what appears to be the dominant room-temperature pathway on supported catalysts. Similarly, most traditional catalyst studies rarely control or report feedwater contents, which has likely contributed to the wide range of reported CO oxidation activities for Au/TiO_2 catalysts and to the difficulties in understanding the key features of the best catalysts. Finally, this new mechanism brings the interpretation of traditional supported catalyst experiments more in line with computational and surface-science studies, which have largely indicated that the key reaction steps occur on Au (*7*, *9*–*14*, *17*, *29*), without direct participation of the support.

REFERENCES AND NOTES

1. M. Cargnello *et al.*, *Science* **341**, 771–773 (2013).
2. A. Corma, P. Serna, *Science* **313**, 332–334 (2006).
3. T. Takei *et al.*, *Adv. Catal.* **55**, 1–126 (2012).
4. B. N. Zope, D. D. Hibbitts, M. Neurock, R. J. Davis, *Science* **330**, 74–78 (2010).
5. C. Della Pina, E. Falletta, M. Rossi, *Chem. Soc. Rev.* **41**, 350–369 (2012).
6. M. Shekhar *et al.*, *J. Am. Chem. Soc.* **134**, 4700–4708 (2012).
7. M. Valden, X. Lai, D. W. Goodman, *Science* **281**, 1647–1650 (1998).
8. A. A. Herzing, C. J. Kiely, A. F. Carley, P. Landon, G. J. Hutchings, *Science* **321**, 1331–1335 (2008).
9. M. S. Chen, D. W. Goodman, *Science* **306**, 252–255 (2004).
10. H. Falsig *et al.*, *Angew. Chem. Int. Ed.* **47**, 4835–4839 (2008).
11. C. Lemire, R. Meyer, S. Shaikhutdinov, H.-J. Freund, *Angew. Chem. Int. Ed.* **43**, 118–121 (2004).
12. G. Mills, M. S. Gordon, H. Metiu, *J. Chem. Phys.* **118**, 4198 (2003).
13. I. N. Remediakis, N. Lopez, J. K. Nørskov, *Angew. Chem. Int. Ed.* **44**, 1824–1826 (2005).
14. L. M. Molina, M. D. Rasmussen, B. Hammer, *J. Chem. Phys.* **120**, 7673–7680 (2004).
15. R. A. Ojifinni *et al.*, *J. Am. Chem. Soc.* **130**, 6801–6812 (2008).
16. D. Widmann, R. J. Behm, *Acc. Chem. Res.* **47**, 740–749 (2014).
17. M. S. Ide, R. J. Davis, *Acc. Chem. Res.* **47**, 825–833 (2014).
18. I. X. Green, W. Tang, M. Neurock, J. T. Yates Jr., *Science* **333**, 736–739 (2011).
19. T. Fujitani, I. Nakamura, *Angew. Chem. Int. Ed.* **50**, 10144–10147 (2011).
20. M. Daté, M. Okumura, S. Tsubota, M. Haruta, *Angew. Chem. Int. Ed.* **43**, 2129–2132 (2004).
21. M. Ojeda, B.-Z. Zhan, E. Iglesia, *J. Catal.* **285**, 92–102 (2012).
22. M. C. Kung, R. J. Davis, H. H. Kung, *J. Phys. Chem. C* **111**, 11767–11775 (2007).
23. M. Haruta, *Faraday Discuss.* **152**, 11–32, discussion 99–120 (2011).
24. J. A. Singh, S. H. Overbury, N. J. Dudney, M. Li, G. M. Veith, *ACS Catal.* **2**, 1138–1146 (2012).
25. W. C. Ketchie, M. Murayama, R. J. Davis, *Top. Catal.* **44**, 307–317 (2007).
26. H. H. Kung, M. C. Kung, C. K. Costello, *J. Catal.* **216**, 425–432 (2003).
27. J. T. Calla, R. J. Davis, *J. Catal.* **241**, 407–416 (2006).
28. C. K. Costello *et al.*, *Appl. Catal. A* **243**, 15–24 (2003).
29. S. Laursen, S. Linic, *Phys. Chem. Chem. Phys.* **11**, 11006–11012 (2009).
30. J. Carrasco, A. Hodgson, A. Michaelides, *Nat. Mater.* **11**, 667–674 (2012).
31. C. G. Long *et al.*, *J. Am. Chem. Soc.* **130**, 10103–10115 (2008).
32. Z.-P. Liu, P. Hu, A. Alavi, *J. Am. Chem. Soc.* **124**, 14770–14779 (2002).
33. L. R. Merte *et al.*, *Science* **336**, 889–893 (2012).
34. A. A. Gokhale, J. A. Dumesic, M. Mavrikakis, *J. Am. Chem. Soc.* **130**, 1402–1414 (2008).
35. L. C. Grabow, A. A. Gokhale, S. T. Evans, J. A. Dumesic, M. Mavrikakis, *J. Phys. Chem. C* **112**, 4608–4617 (2008).
36. G. M. Veith, A. R. Lupini, N. J. Dudney, *J. Phys. Chem. C* **113**, 269–280 (2009).

ACKNOWLEDGMENTS

We gratefully acknowledge the U.S. National Science Foundation (grants CBET-1160217, CHE-1012395, and CHE-1300619) and the U.S. Department of Energy (NSF/DOE CBET-1258688) for financial support of this work. We also thank R. Rioux (Pennsylvania State University) and Z. Tonzetich (University of Texas at San Antonio) for assistance with transmission electron microscopy and thermogravimetric analysis measurements, respectively. Additional financial support was provided to L.C.G. and H.A.D. through a University of Houston New Faculty Grant. Use of the computational resources at the Center for Nanoscale Materials was supported by the U.S. DOE, Office of Science, Office of Basic Energy Sciences, under contract no. DE-AC02-06CH11357. This work also used the Extreme Science and Engineering Discovery Environment (XSEDE, supported by NSF grant OCI-1053575) and the Kraken computing resource at the National Institute for Computational Sciences (supported by NSF grants 0711134, 0933959, 1041709, and 1041710 and the University of Tennessee). We acknowledge the Texas Advanced Computing Center (TACC) at The University of Texas at Austin for providing high-performance computing resources that have contributed to the research results reported in this paper. Additional computational resources were provided by the Center for Advanced Computing and Data Systems (CACDS, formerly Texas Learning and Computation Center, TLC^2) and the Research Computing Center (RCC) at the University of Houston.

SUPPLEMENTARY MATERIALS

www.sciencemag.org/content/345/6204/1599/suppl/DC1
Materials and Methods
Supplementary Text
Figs. S1 to S12
Scheme S1
Tables S1 to S8
Movie S1

13 May 2014; accepted 8 August 2014
Published online 4 September 2014;
10.1126/science.1256018

PLANT ECOLOGY

Environmental filtering explains variation in plant diversity along resource gradients

Etienne Laliberté,[1]* Graham Zemunik,[1] Benjamin L. Turner[2]

The mechanisms that shape plant diversity along resource gradients remain unresolved because competing theories have been evaluated in isolation. By testing multiple theories simultaneously across a >2-million-year dune chronosequence in an Australian biodiversity hotspot, we show that variation in plant diversity is not explained by local resource heterogeneity, resource partitioning, nutrient stoichiometry, or soil fertility along this strong resource gradient. Rather, our results suggest that diversity is determined by environmental filtering from the regional flora, driven by soil acidification during long-term pedogenesis. This finding challenges the prevailing view that resource competition controls local plant diversity along resource gradients, and instead reflects processes shaping species pools over evolutionary time scales.

For decades, ecologists have sought to understand patterns in terrestrial plant diversity along environmental gradients (*1*). Prominent theories emphasize resource competition as a key driver of diversity (*2*–*4*). Alternatively, it has been proposed that variation in local plant diversity along gradients reflects the filtering of species that are poorly adapted to local environmental conditions (*5*–*7*), highlighting the importance of long-term evolutionary processes in shaping species pools and present-day patterns of plant diversity. These competing hypotheses have been considered in isolation, and further progress can be made only by considering the